Integrative and Comparative Biology

Integrative and Comparative Biology, volume 55, number 4, pp. 740–752
doi:10.1093/icb/icv015

Society for Integrative and Comparative Biology

SYMPOSIUM

Simulations of Unsteady Aquatic Locomotion: From Unsteadiness in Straight-Line Swimming to Fast-Starts

Iman Borazjani[1]

Mechanical and Aerospace Engineering Department, University at Buffalo, State University of New York, Buffalo, NY 14260, USA

From the symposium "Unsteady Aquatic Locomotion with Respect to Eco-Design and Mechanics" presented at the annual meeting of the Society for Integrative and Comparative Biology, January 3–7, 2015 at West Palm Beach, Florida.

[1]E-mail: iman@buffalo.edu

Synopsis Unsteady aquatic locomotion is not an exception, but rather how animals often swim. It includes fast-starts (C-start or S-start), escape maneuvers, turns, acceleration/deceleration, and even during steady locomotion the swimming speed fluctuates, i.e., there is unsteadiness. Here, a review of the recent work on unsteady aquatic locomotion with emphasis on numerical simulations is presented. The review is started by an overview of different theoretical and numerical methods that have been used for unsteady swimming, and then the insights provided by these methods on (1) unsteadiness in straight-line swimming and (2) unsteady fast-starts and turns are discussed. The swimming speed's unsteady fluctuations during straight-line swimming are typically less than 3% of the average swimming speed, but recent simulations show that body shape affects fluctuations more than does body kinematics, i.e., changing the shape of the body generates larger fluctuations than does changing its kinematics. For fast-starts, recent simulations show that the best motion to maximize the distance traveled from rest are similar to the experimentally observed C-start maneuvers. Furthermore, another set of simulations, which are validated against measurements of flow in experiments with live fish, investigate the role of fins during the C-start. The simulations showed that most of the force is generated by the body of the fish (not by fins) during the first stage of the C-start when the fish bends itself into the C-shape. However, in the second stage, when it rapidly bends out of the C-shape, more than 70% of the instantaneous hydrodynamic force is produced by the tail. The effect of dorsal and anal fins was less than 5% of the instantaneous force in both stages, except for a short period of time (2 ms) just before the second stage. Therefore, the active control and the erection of the anal/dorsal fins might be related to retaining the stability of the sunfish against roll and pitch during the C-start. At the end, the needed future developments in the computational front and their possible applications on investigating stability during unsteady locomotion are discussed.

Introduction

Unsteady aquatic locomotion is not the exception, but the typical mode of locomotion in aquatic environments. Unsteady aquatic locomotion is needed during acceleration (Tytell 2004), deceleration (Niiler and White 1969), turning and maneuvering (Weihs 1972; Blake et al. 1995; Muller et al. 2000; Fish and Nicastro 2003; Maresh et al. 2004; Parson et al. 2011), burst and coast (Videler and Weihs 1982; Blake 1983; Stöcker and Weihs 2001; Burnett et al. 2014), fast-starts for capturing prey (Webb 1984; Harper and Blake 1991; Canfield and Rose 1993), avoidance of predators (Walker et al. 2005), mating (Wilson et al. 2010), and other activities. In fact, even during steady, straight-line swimming, the swimming speed is not constant and fluctuates, as will be discussed in the Unsteadiness in steady swimming section. Reviewing all the studies of unsteady locomotion is not possible in a single paper. Therefore, this article is focused on unsteadiness (fluctuations) during steady swimming and fast starts with emphasis on the insights obtained through theoretical and numerical studies. The theoretical and numerical studies can complement experimental studies by providing detailed description of the phenomena, e.g., 3D flow field, that are

Advanced Access publication April 17, 2015

difficult to obtain experimentally, or by testing/simulating hypothetical cases, e.g., what if a sunfish did not have a tail during the C-start, as an inverse problem to answer fundamental questions related to why certain biological features appear in nature.

The motion of the body during fast-starts is quite different than during steady swimming. In steady swimming, the body's motion can be closely approximated by a backward traveling wave (Gray 1933; Videler and Hess 1984). In contrast, in fast-starts, the fish typically bends its body into a C-shape (stage 1) and then rapidly bends out of the C-shape (stage 2), which might be followed by one or more beats of the tail (Weihs 1973). The kinematics of C-starts has been studied from several viewpoints, e.g., see Domenici and Blake (1991, 1993), Spierts and Leeuwen (1999), and the review by Domenici and Blake (1997). Fast-start kinematics has been used to calculate the acceleration of the center of mass of the fish and the forces generated during this behavior (e.g., see Webb and Skadsen 1980; Webb 1984; Harper and Blake 1988, 1991; Domenici and Blake 1991, 1993; Webb et al. 1996, among others; Domenici and Batty 1997; Bergstrom 2002; Domenici et al. 2004). The digitization and numerical differentiation error of such calculations has been discussed (Harper and Blake 1989; Walker 1998).

The acceleration of the fish's center of mass is the result of all forces acting on the center of mass, i.e., the total hydrodynamic force can be calculated through acceleration, but how much each part of the body/fins contributes to the total hydrodynamic force cannot be calculated. Therefore, the muscle and hydrodynamic forces need to be estimated for different parts of body/muscle groups to gain such insights. The C-start has been extensively studied in terms of muscle activity (Jayne and Lauder 1993; Wakeling and Johnston 1998, 1999; Westneat et al. 1998; Wakeling et al. 1999; Ellerby and Altringham 2001; Tytell and Lauder 2002), and neural control (Fetcho 1991; Zottoli et al. 1995; Eaton et al. 2001; Tytell and Lauder 2002; Koyama et al. 2011), and will not be reviewed in this article. The theoretical models, numerical simulations, and experimental wake measurements have been performed to estimate the hydrodynamic forces during the C-start (Weihs 1973; Wolfgang et al. 1999; Tytell and Lauder 2008; Borazjani et al. 2012; Borazjani 2013; Li et al. 2014). These theoretical models and computational methods are reviewed briefly in the Theoretical models and computational techniques for unsteady swimming section, and the insights provided by these methods are discussed in the Insights from theoretical and computational studies section. In the Unsteadiness in steady swimming section, the unsteadiness during steady swimming and the parameters affecting fluctuations in swimming speed, e.g., Reynolds number (Re), body shape, and kinematics, are discussed. In the Fast-starts and turning maneuvers section, the insights from theoretical and numerical work on fast start and turning maneuvers are reviewed and the role of fins during C-start is discussed. Finally, different methods are compared, their suitability for different types of problem is discussed, and future directions are suggested in the Discussions and future directions section.

Theoretical models and computational techniques for unsteady swimming

In this section, a brief overview of the theoretical and computational methods, which can be used to investigate unsteady aquatic locomotion, is provided. The theoretical models based on elongated-body theory (EBT) are discussed in the Elongated body theory section, followed by the inviscid-vortex methods in the Inviscid methods (unsteady, vortex-panel methods) section. Finally, the techniques of computational fluid dynamics (CFD), which are capable of simulating flows with unsteady body-movements of the swimmers, are discussed in the Computational fluid dynamics section.

Elongated body theory

The so-called slender-body, or EBT, pioneered by (Lighthill 1960, 1969, 1970, 1971) and (Wu 1960, 1971a, 1971b, 1971c)—see the recent review by Wu (2011), is one of the first approaches used to identify the physical mechanism behind aquatic locomotion. EBT has provided the first estimates for power P and thrust T, leading to a simple formula for efficiency η for steady swimming as $\eta = 1/2(1 + U/V)$, where U is the speed of swimming and V is the velocity of the backward-traveling wave of the body (Lighthill 1960). The EBT assumes the slenderness of the body, i.e., the length of the body L is much larger than its depth b, $b/L \ll 1$ (Lighthill 1960). Furthermore, it assumes that the fluid is inviscid with no vortex shedding, i.e., the boundary layer enveloping the fish is so thin that its thickness can be neglected for evaluation of thrust T and power P of fish locomotion (Lighthill 1970; Wu 1971a, 2011). This is a good assumption at high $\mathrm{Re} = UL/\vartheta$ (where ϑ is the kinematic viscosity of the fluid), which represents the ratio of inertial to viscous forces in the flow, if the flow does not separate. Nevertheless, these methods are known to

overestimate the forces and efficiency by several folds because of their simplifying assumptions (Lighthill 1970).

Wu (1971a, 1971c) extended the EBT to handle variable rectilinear speeds U(t) of two-dimensional flexible plates, and applied it to find the initial optimum shape of the plate for constant acceleration from rest. Weihs (1972) extended Lighthill's EBT for large-amplitude linear movements of slender bodies in inviscid fluids (Lighthill 1971) to turning maneuvers. Because of the inviscid assumption of this theory, only the changes in momentum due to the motions perpendicular to the fish's spinal column are considered, and the forces due to tangential movements are neglected (Weihs 1972). The forces acting on the fish are equal to the change of the momentum of the fish itself (Weihs 1972). These forces arise from changes in the momentum of the water surrounding the fish, and from the wake caused by its passage (Weihs 1972). The slender-body assumption only takes the changes in lateral momentum into account, and to treat the contributions of each transverse section of the fish independently (Weihs 1972). In an inviscid fluid, the changes in momentum in the wake can be represented by the summation of forces due to the acceleration of the adjacent fluid to a body (added mass force) or due to the circulatory (lift) forces created by differences in velocity over different sides of fins/body sections similar to airplane wings (Weihs 1972):

$$\vec{F} = \underbrace{\frac{\partial}{\partial t}\int mw\vec{n}\,da}_{\text{added mass force}} + \underbrace{\sum_{i=1}^{k}\vec{L_i}}_{\text{circularoy (lift) force}} \quad (1)$$

where $\vec{F}$ is the hydrodynamic force, t is the time, $\vec{n}$ is the unit vector perpendicular to the backbone, da is the small element along the direction of the backbone, m is the added mass of a cross-section, and w is the velocity component perpendicular to the centerline at that cross-section, and $\vec{L_i}$ is the force caused by the circulatory (lift) forces from fin i, and k is the number of fins. The first term in Equation (1) can be considered as the rate of change (time derivative) of momentum (mass times velocity) due to the added mass. Note that if m in Equation (1) were constant, then the first term would reduce to added mass times the acceleration dw/dt. The added mass of a cross-section is mainly dependent on the dorsoventral depth of the cross-section s and the density of the fluid ρ (Weihs 1972):

$$m = \frac{1}{4}\pi\rho s^2\beta, \quad (2)$$

where β is a coefficient sufficiently close to unity for various configurations of the cross-section and for gradual changes in cross-section and lateral velocity along the backbone (Lighthill 1970). The circulatory forces $\vec{L_i}$ can be calculated by the classical methods of aerodynamics for each fin, e.g. (Weihs 1972):

$$L_i = \frac{1}{2}\rho v_i^2 A_i \;\; C_{L,\alpha}\alpha_i, \quad (3)$$

where A_i is the area of the fin, v_i is the velocity of the center of pressure of the fin, and $C_{L,\alpha}$ is the lift coefficient with the angle of attack, and α_i is the angle of attack (measured between the fin's zero lift line and the direction of motion). $C_{L,\alpha}$ is the only quantity in Equation (3), which depends on the shape of the fin. Weihs (1972) calculated $C_{L,\alpha}$ by means of well-known methods (Robinson and Laurmann 1956) for steady flow, and the correction for unsteady flow was obtained by the indicial method (Lomax 1960).

By calculating the added mass and lift forces from Equations (2) and (3), respectively, for different sections of the fish, Weihs (1972) calculated the total reactive force on the fish's body during turns. Weihs (1973) applied his method to study fast-starts, and Frith and Blake (1991) used this method to investigate the fast-start of the northern pike.

Inviscid methods (unsteady, vortex-panel methods)

Inviscid-flow methods can be applied to any complex geometry with arbitrary motions without the assumption of slenderness of the previous theoretical work. Inviscid-flow methods are attractive because of their low computational costs relative to the CFD (section Computational fluid dynamics). However, they cannot capture flow separation and dynamic interaction between vortices in fish wakes due to their assumption of inviscid flow. The main reason for low computational costs of inviscid-flow methods is that the flow equations can be simplified to reduce the mathematical and computational complexity (Wolfgang et al. 1999; Kanso et al. 2005; Kanso 2009). In fact, assuming inviscid, irrotational flow, there exists a velocity potential φ which satisfies the Laplace equation for conservation of mass for incompressible flows, i.e., the equations governing flow reduce to the Laplace equation $\nabla^2\varphi = 0$. Furthermore, the Laplace equation over the complete volume of a domain reduces to a surface integral on the boundaries of the domain using the divergence theorem (Katz and Plotkin 2001). Because of the linearity of the Laplace equation, several simple solutions can be superimposed to obtain more complex solutions, e.g., the potential vortex satisfies the

Laplace equation, and by combining several potential vortices, flows over more complex geometries can be obtained (vortex-panel method). The unsteady, vortex-panel method (Hess and Smith 1967; Katz and Plotkin 2001) can be used to obtain the forces during unsteady motions. In these methods, the geometry, i.e., the fish's body and the wake, is covered by vortex sheets whose strength γ varies with location such that the combined action of incoming flow and vortex sheets makes the cross section of the body a streamline of the flow. The midpoint of each panel is a control point at which the boundary condition is applied; i.e., at each control point, the component velocity, induced by the vortex sheets and the free flow, in the normal direction to the panel surface is equal to the normal velocity of the panel wall (no flux condition):

$$V_{\infty,n} + V_n = V_{w,n}, \tag{4}$$

where $V_{\infty,n}$ is the normal component of the swimming velocity V_∞, $V_{w,n}$ is the normal component of the velocity of the panel's wall, and V_n is the normal component of the induced velocity by vortex panels:

$$V_n = \frac{\partial}{\partial n_i}[\varphi(x_i, y_i, z_i)], \tag{5}$$

where φ is the velocity potential at ith panel control point (x_i, y_i, z_i) due to all vortex panels (both body and wake panels). Writing Equation (4) for all of the panels and applying the Kutta condition at the trailing edge provide a system of equations that can be solved to obtain the vortex strength γ of each panel. At any instant of time, the strength of any previously shed wake is known, except for the recently shed vortices at the trailing edge. The unknown strengths of the newest part of the wake sheet are addressed through the Kutta condition (Wolfgang et al. 1999). By knowing the vortex strength γ, the velocity and velocity potential at each panel is known. Therefore, the pressure at each panel can be obtained using the unsteady Bernoulli equation, neglecting the potential energy:

$$\frac{p_\infty - p}{\rho} = \frac{|V|^2}{2} + \frac{\partial \varphi}{\partial t}, \tag{6}$$

where p_∞ is the free-stream pressure, p is the static pressure on the surface, ρ is the density of the fluid, and V is the velocity. After obtaining the pressure field, the forces will be calculated by integrating the pressure over the surface of the fish's body. Such unsteady, vortex-panel method has been used to investigate the turning maneuver of a giant danio (Wolfgang et al. 1999).

Computational fluid dynamics

The governing equations for the flow around aquatic swimmers during unsteady locomotion are the unsteady, incompressible Navier–Stokes equations. These equations are typically discretized and solved over a finite number of discrete points in space, i.e., the grid. The main challenge involved in simulations of aquatic swimmers is handling complex geometries and their motion (moving-boundary problem). For grid-based techniques, there are two main classes of methods for handling moving boundaries: (1) boundary-conforming and (2) non-boundary-conforming (fixed grid) methods. In boundary-conforming methods, the grid moves with the moving boundary, and the governing equations need to be modified to incorporate the grid velocities, i.e., the Arbitrary Lagrangian–Eulerian (ALE) formulation (Donea et al. 2004). In non-boundary-conforming methods, in contrast, the grid is fixed and the effects of the boundary's motion need to be transferred onto the grid nodes in the vicinity of the moving boundary. There are different non-boundary-conforming methods, e.g., immersed-boundary method (Mittal and Iaccarino 2005), cut-cell method (Ji et al. 2008), level-set method (Sethian 1999), and Brinkman penalization method (Angot et al. 1999; Coquerelle and Cottet 2008).

Boundary-conforming methods can preserve high resolution near the moving boundaries, but may result in highly skewed grids when the deformations are large. To improve the mesh quality when the deformations are large, remeshing might be necessary, which can be computationally expensive. The non-boundary-conforming methods do not need remeshing because the grid is fixed, but they require additional work in terms of identifying the grid nodes adjacent to the moving boundaries and of transferring the effects onto those nodes.

The ALE method has been used to investigate unsteady maneuvers of a larval fish (Li et al. 2012, 2014). In this method a multi-block, curvilinear grid is used to discretize the computational domain, and the equations are solved using an artificial compressibility method. One curvilinear grid block that conforms to the fish's body and its movements (inner block) is placed over another grid block (background grid). The far-field boundary conditions are applied on the background grid, while the no-slip boundary conditions are applied on an inner block that moves with the fish's body (Li et al. 2012). The boundary conditions at the interface of two grids and their overlapping region is reconstructed through interpolation (Li et al. 2012).

Non-boundary-conforming methods do not require mesh movements, but need to transfer the effects of moving boundaries to the grid points adjacent to those boundaries. In the original immersed-boundary method, pioneered by Peskin (1972, 1977; Peskin and McQueen 1980, 1989), which has been applied to aquatic locomotion (Fauci and Peskin 1988), the presence of moving boundaries in the flow is accounted for by adding forcing terms to the right-hand side of the Navier–Stokes equations on the nodes adjacent to the moving boundaries. These forcing terms are smeared over several grid nodes using a delta function for stability, i.e., the interface is diffused over several grid nodes, which requires additional resolution near the boundary. However, due to high costs, the majority of simulations using this method has been two-dimensional (Tytell et al. 2010; Bhalla et al. 2013).

To overcome the limitations of diffuse interface in the classic immersed-boundary method, a number of sharp-interface, immersed-boundary methods have been developed (Borazjani et al. 2008; Mittal et al. 2008). In these methods, sharp-interface is maintained by reconstructing the boundary conditions at the grid nodes that are in the immediate vicinity of the moving boundaries through interpolation along the local normal to the boundary (Gilmanov and Sotiropoulos 2005; Mittal et al. 2008). The nodes adjacent to the immersed boundaries need to be identified at each time instant that the boundary is moving. Borazjani et al. (2008) used an efficient ray-tracing algorithm to identify these nodes.

Gazzola et al. (2012) used a remeshed-vortex method (Koumoutsakos and Leonard 1995; Eldredge 2006; Gazzola et al. 2011), which solves the Navier–Stokes equations through Lagrangian particle advection followed by remeshing of particles (reordering of particles' locations onto a uniform grid while interpolating the old vorticity onto new locations of particles), along with the Brinkman penalization (Coquerelle and Cottet 2008) method to simulate the fast-start behavior of larval fish. The penalization term added to the Navier–Stokes equations approximates the no-slip-boundary condition at the body interface, and can be viewed as the Lagrangian counterpart of the forcing term in the classical immersed-boundary method. The unsteady maneuvering of fish was also simulated using the adaptive version of this method (Gazzola et al. 2014).

Insights from theoretical and computational studies

In this section, the insights obtained through theoretical models and numerical simulations are reviewed for fluctuations in swimming speed during steady swimming (section Unsteadiness in steady swimming) and fast starts (section Fast-starts and turning maneuvers).

Unsteadiness in steady swimming

In self-propelled simulations of swimmers using different CFD techniques (Borazjani and Sotiropoulos 2010; Li et al. 2012; Borazjani and Daghooghi 2013), the swimmer is initially at rest but starts accelerating as it starts to undulate. The velocity of swimming increases until it reaches the quasi-steady state at which the average swimming speed remains constant—e.g., see Fig. 1A. However, there are fluctuations around the mean value, even when the swimmer reaches a quasi-steady state, e.g., see Fig. 1A, Fig. 7 of Li et al. (2012), or Fig. 3 of van Rees et al. (2013). In fact, this has been observed in experiments as well. Observations of swimming eels have revealed about 10% (Muller et al. 2001) or 4% (Tytell and Lauder 2004) fluctuations about the mean velocity, while swimming mullets have been found to exhibit fluctuations of velocity of more than 20% of the mean (Muller et al. 1997; Nauen and Lauder 2002). Furthermore, the swimming speed of zebra fish larvae at $\mathrm{Re} \approx 300$ fluctuates between 14 and 24 Ls^{-1} (L is the length of a fish) (Muller et al. 2008), while for an adult eel swimming at $\mathrm{Re} \approx 10{,}000$ the swimming speed fluctuates within a much narrower range between 0.9 and 1.1 of the average velocity (Muller et al. 2001; Tytell and Lauder 2004).

It is not clear if the above difference in fluctuations is because of the shape of the body, kinematics, or Reynolds number. Using a sharp-interface, immersed-boundary method, Borazjani and Sotiropoulos (2010) separated the effects of body shape and kinematics in their simulations by reconstructing virtual swimmers that have the same kinematics but different shapes of the body, and vice versa (Fig. 1), and carried out simulations at three Re of about 300, 4000, and $\mathrm{Re} \to \infty$. Figure 1B plots the root-mean-squared (rms) of fluctuations in velocity over the average velocity for swimmers with different bodies, kinematics, and Re (Borazjani and Sotiropoulos 2010). Several trends are observed (Fig. 1B): (1) For a given swimmer and kinematics, the fluctuations decrease as Re increases; (2) under similar Re, the mackerel's body shape creates higher fluctuations in velocity than does lamprey's body shape; and (3) under similar Re and body shape, the lamprey's kinematics creates lower fluctuations than does the mackerel's kinematics. Furthermore,

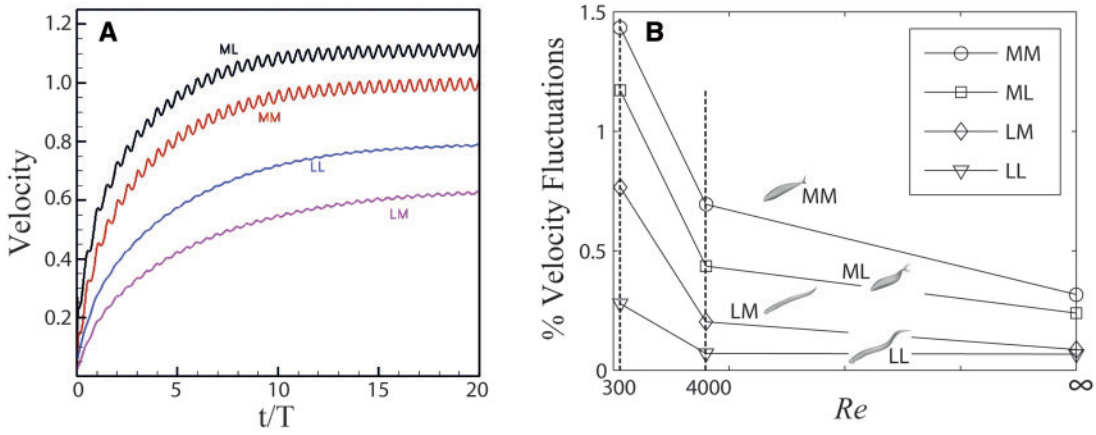

Fig. 1 (**A**) The non-dimensional velocity is plotted in time *t* (divided by tail-beat duration T) for different swimmers at Re 300. It can be observed that the swimming speed increases from zero until it reaches the quasi-steady state, but even in quasi-steady state it is not constant and fluctuates around an average value. (**B**) The percentage of room-mean-squared (rms) of the velocity fluctuations over average velocity during quasi-steady state at different Re for different swimmers. MM, mackerel body and mackerel kinematics; ML, mackerel body and lamprey kinematics; LM, lamprey body and mackerel kinematics; LL, lamprey body and lamprey kinematics. Adopted from Borazjani and Sotriopoulos (2010). (This figure is available in black and white in print and in color at *Integrative and Comparative Biology* online.)

it can be observed in Fig. 1B that in these simulations, body shape has a greater effect on fluctuations than does the Re, and the least effect is from kinematics, e.g., at Re 4000 and with mackerel kinematics changing the shape of the body from mackerel to lamprey reduced fluctuations by 75%, whereas with the mackerel body changing the kinematics from mackerel to lamprey reduced the fluctuations by about 35%. For the mackerel (MM swimmer in the figure), changing Re from 300 to 4000 reduces the fluctuations by 52%, and from 4000 to ∞ by 44%, i.e., more than the effect of kinematics but less than the effect of body shape. It can be observed that the change in fluctuations from Re 300 to 4000 is much larger than the change from Re 4000 to ∞., i.e., as Re approaches zero the fluctuations in velocity increase even faster. In fact, for smaller animals that swim at lower Re, e.g., larval fish (Muller et al. 2008) or copepods (Strickler 1975; Yen and Strickler 1996; van Duren and Videler 2003), the fluctuations are higher. For the copepods, the velocity increases and suddenly decreases after the hop. The simulations of a copepod (Borazjani et al. 2010) also show that the force coefficients on the body of the copepod increase (both during power strokes and return strokes of the appendages) as the Re decreases, which is in agreement with the current trend.

The reasons behind these trends might not be readily clear. The Re can be viewed as the ratio of inertial to viscous forces. As Re decreases, the proportion of the inertia, which tends to keep the swimmer's speed constant, to viscous force, i.e., skin friction, which tends to reduce the swimmer's speed, decreases. Therefore, the swimmer decelerates faster and requires larger thrust force, which leads to higher fluctuations. The reason for a lamprey's (eel-like) kinematics always generating lower fluctuations relative to the mackerel-like kinematics is due to the shorter wavelength and higher amplitudes of the lamprey's traveling wave, which always accelerates the adjacent fluid backward by some part of the body, i.e., the generation of force is smoother. The reason that the mackerel's body shape increases fluctuations more than do kinematics or Re is probably related to the recently found leading-edge vortices that are generated on the fish's tail (Borazjani and Daghooghi 2013). The leading-edge vortices, generated on the mackerel's tail, create a large peak in the force as they are generated, which will vanish when these vortices are diminished, i.e., a highly oscillatory force is generated by the mackerel's body that creates oscillatory acceleration, and consequently, oscillations in velocity. A lamprey's tail does not have a sharp leading edge similar to the mackerel's, i.e., no leading-edge vortex will be generated on the lampreys' tail.

Fast-starts and turning maneuvers

The early work on fast-starts and turns was pioneered by the EBT model of Weihs (1972, 1973). Weihs (1972) observed the turning maneuver of a goldfish (*Cyprinus auratus*) and a rudd (*Cyprinus erythrophthalmus*), finding several distinct stages: (1) the initial swimming; (2) turning by bending

the body into an arc; and (3) bending out of the arc and swimming in the new direction. The total forces and moments obtained by EBT during the turning maneuvers were about 30% lower than the observed change in momentum, likely due to numerical errors, uncertainties of measurement, and viscous forces, which are ignored in this theory (Weihs 1972). Wolfgang et al. (1999) used an unsteady-panel method to simulate the flow on the 2D midplane of giant danio during a 60° turn. The flow field generated by this method near the caudal fin showed qualitative similarities to the experimental measurements.

Weihs (1973) applied his theory to fast starts. Again, he identified several stages that he named: the preparatory stage (stage 1) in which the body is arced into a C-shape; the propulsive stage (stage 2) in which the body bends out of the C-shape; and the final stage (stage 3), which involves continuous swimming or coasting. Based on his EBT analysis, the optimum motion during fast starts to maximize forces is when the caudal fin moves at fast speeds perpendicular to the direction of motion, while being at low angle of incidence (Weihs 1973). Recently, Gazzola et al. (2012) studied the C-start of larval fish using simulations with the remeshed vortex and Brinkman penalization method at moderate Reynolds numbers with an evolutionary optimization for the kinematics. They found that the best motions to maximize the distance traveled from rest are similar to the experimentally observed C-start maneuvers.

Borazjani et al. (2012) simulated a sunfish whose geometry and body motion was reconstructed, based on the experimental measurements of a C-start maneuver (Tytell and Lauder 2008). The simulations were validated against the measurements of flow, which could reproduce all the experimentally observed features of flow such as the three jet-flows (Borazjani et al. 2012)—see Fig. 2A, B. Furthermore, these simulations revealed, for the first time, the 3D wake structure consisting of multiple connected vortex loops, through which the three jets flow (Fig. 2C). Furthermore, the forces calculated on the basis of the measured and simulated flow on the 2D midplane of the fish show good agreement (Fig. 3A). Comparing the forces calculated on the basis of the 2D flow field (Fig. 3A) and the 3D flow field (Fig. 3B) and observing their differences shows the need for calculating the forces based on 3D flow and pressure fields.

Li et al. (2012) prescribed the body motion of a zebra fish larva from experimental observations in their ALE simulations, and calculated the motion of the center of mass. The calculated motion of the center of mass resembled the experimental one, and the maximum deviation occurred during the preparatory stroke. Nevertheless, the simulations captured all the features of flow observed in experiments (Li et al. 2012). More recently, Li et al. (2014) investigated the effect of previously shed wake on the C-start by artificially removing the previously shed wake and comparing the trajectory of the center of mass with the simulations when the wake was not removed. Their simulations show that the previously shed wake can reduce the fish's turning angle by 5°, but it did not significantly affect the required power or the acceleration in the direction of the escape trajectory (Li et al. 2014).

It can be observed in Fig. 3B that the forces for $Re = \infty$ have fluctuations about the forces for simulations of $Re = 4000$, but they are similar and follow the same trend, i.e., in the high Re regimes ($Re \gg 1$) the forces during C-start are not affected by Re. However, if the Re is further reduced, e.g., reducing it to $Re = 1$, there is a large difference in the forces, i.e., the performance of C-start degrades as Re is decreased. This is consistent with the finding of Danos and Lauder (2012) that increasing the viscosity by 20 times did not affect the timing of the stages of C-start, but decreased the maximum velocity and displacement of the center of mass. The numerical simulations of Li et al. (2014) also show decrease in the displacement of the center of mass, and also changes the final direction of escape direction by the fish larva.

Role of fins

The EBT model of Weihs (1973) predicts that the caudal fin generates the majority of hydrodynamic force during the C-start because the highest acceleration occurs in that region, i.e., high added mass force. Webb (1977) studied the effect of different fins on live fish by measuring the average acceleration of fish whose fins are amputated in eight different ways (Webb 1977): control (pelvic rays amputated); dorsal fin; anal fin; dorsal lobe of caudal fin and ventral lobe of caudal fin; ventral lobe of caudal fin and anal fin; dorsal and ventral lobes of caudal fin; and both caudal-fin lobes and anal fin. The series represents a progressive reduction in the area of fins and of the body, as well as reduction in the areas where lateral movements are largest (Webb 1977); thus, the acceleration of fish should decrease progressively in the series according to the EBT. However, in contrast to the theory, the reduction in performance of C-start caused by the removal of

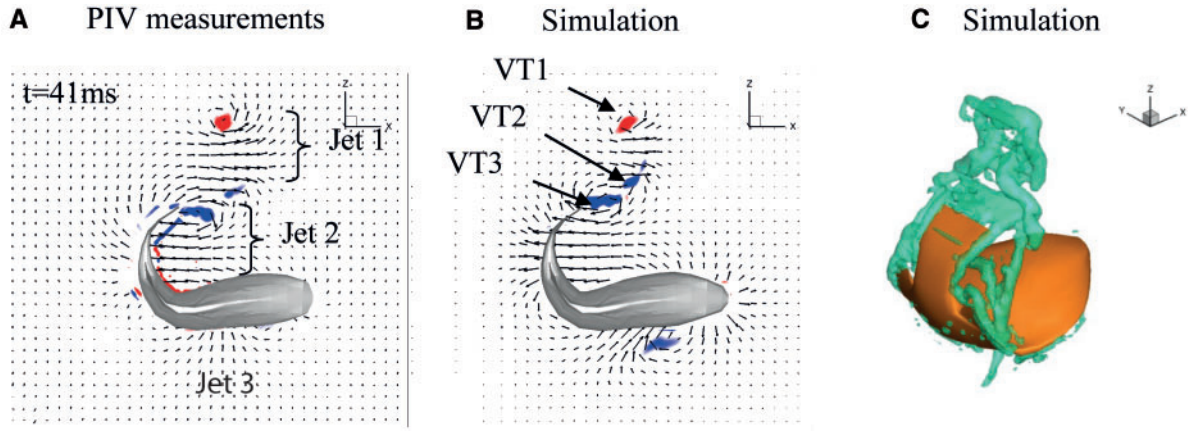

Fig. 2 The flow in the midplane of the sunfish visualized by velocity vectors and contours of non-dimensional vorticity at $t = 41$ ms obtained from PIV measurements (**A**) and the simulation (**B**). The three dominant jet flows are labeled in (A) and the vortices in (B). (**C**) Three-dimensional vortical structures are visualized by the iso-surfaces of the q-criterion from the simulations. Adopted from Borazjani et al. (2012).

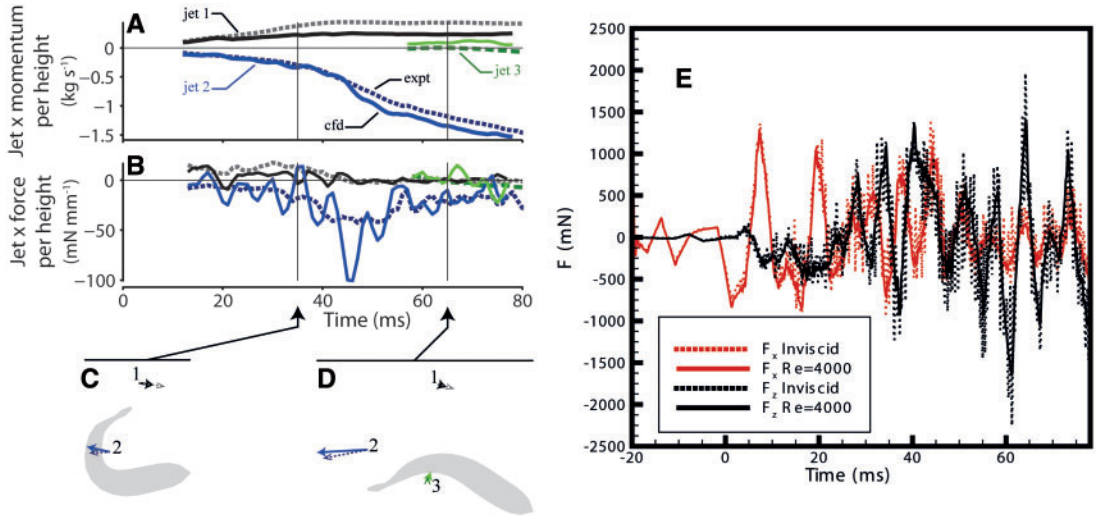

Fig. 3 (**A–D**) Two-dimensional estimates of force and momentum from CFD and experiments (from Tytell and Lauder 2008) and (**E**) the three-dimensional estimates of forces from CFD. CFD and experimental results match well, although the CFD results have larger fluctuations. Comparing the estimates of force based on two-dimensional (B) and three-dimensional (**E**) flow field shows the need for calculations of 3D flow. Momentum (A) and force (B) in the *x* direction are estimated in the same way in the horizontal midline plane for each jet. The current CFD results are shown with solid lines, and previous experimental results are indicated by dashed lines. Panels C and D show the direction and magnitude of the momentum in each jet at two and three example points in time, respectively, with the silhouette of the fish body shown in gray. Adopted from Borazjani et al. (2012). (This figure is available in black and white in print and in color at *Integrative and Comparative Biology* online.)

dorsal/anal fins was not statistically significant (less than 5%), while the removal of the caudal fin caused a statistically significant reduction in the performance (more than 5%). This might be because trout were used in these experiments; they do not have enlarged dorsal and anal fins and the dorsal fin is located away from the tail. Nevertheless, no definitive conclusions on the effect of removal of the dorsal and anal fins could be made due to the statistically insignificant differences (Webb 1977).

Borazjani (2013), using a sharp-interface, immersed-boundary method, tackled this problem by simulating sunfish whose fins were removed or erected, but moving the same as the sunfish with all the fins intact (Borazjani et al. 2012)—see Fig. 4. It can be observed in Fig. 4 that only the removal of the tail generates a large deviation from the forces generated by the original sunfish. In fact, more than 70% of the instantaneous force is generated by the tail during the second stage (Fig. 4).

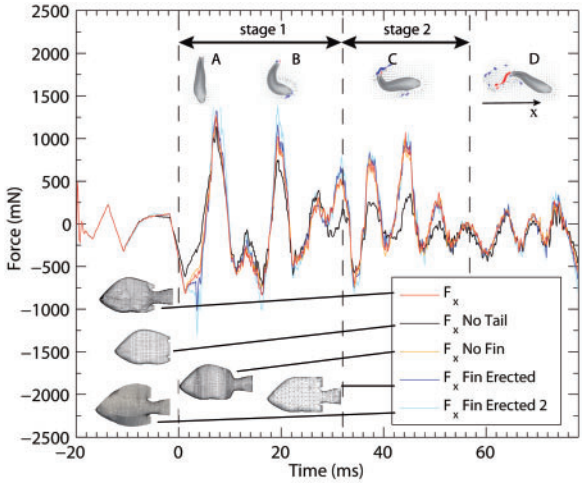

Fig. 4 Force in the escape (x) direction for swimmers with different fins removed/erected. The insets show the body shape and the flow of the sunfish with no tail at t of 5 ms (**A**), 21 ms (**B**), 41 ms (**C**), and 71 ms (**D**). Adopted from Borazjani (2013). (This figure is available in black and white in print and in color at *Integrative and Comparative Biology* online.)

However, the forces generated by the sunfish whose anal/dorsal fins were removed or erected are quite similar to the original one (less than 5% difference at any instant in time except for a short period of time [2 ms] just before the second stage). This is in contrast with the estimate by Tytell and Lauder (2008) that about 37% of the momentum was contributed by anal and dorsal fins by the end of stage 2. The discrepancy between these estimates can be explained by several factors: (1) the estimate by Tytell and Lauder (2008) is made by calculating the momentum in the wake on the 2D planes that passes through the anal and dorsal fins, but because of the three-dimensionality of the flow some of the momentum in these planes might have been contributed by the tail or the body; (2) as discussed in Fig. 3 the estimates of force from the 2D flow field can have inaccuracies; and (3) the simulations did not take into account the exact motion of the anal and dorsal fins, e.g., the traveling wave that passes through these fins, as reported by Chadwell et al. (2012a). Nevertheless, even if the anal/dorsal fin do not contribute much to the total hydrodynamic force, they are actively controlled during the C-start as shown through measurements of muscle activity (Jayne et al. 1996; Standen and Lauder 2005; Lauder et al. 2007; Chadwell and Ashley-Ross 2012; Chadwell et al. 2012a, 2012b). It is hypothesized that the active control of these fins is related to controlling the stability of the fish during the C-start, rather than to the generation of hydrodynamic forces (Borazjani 2013).

During the C-start the fish mainly changes its orientation around the yaw-axis, but not rotating around the roll-axis or pitch-axis, i.e., remains in the horizontal plane—see Fig. 5 for the definition of roll, pitch, and yaw. To be stable during C-start, the angular acceleration around the pitch and roll axes should be small, i.e., $\ddot{\theta}_i = M_i/I_i \ll 1$, where $\ddot{\theta}_i$, M_i, and I_i are angular acceleration, torque, and the moment of inertia around axis i (pitch or roll), respectively. The erection and movements of the fins might stabilize in two different ways (Borazjani 2013): (1) passively by increasing the moment of inertia I_i around the pitch and roll axes and (2) actively by counteracting the torque created by other parts of the body and that lowers the total torque M_i.

Discussions and future directions

The main methods for simulating unsteady aquatic locomotion were reviewed in the Theoretical models and computational techniques for unsteady swimming section. Each of these methods has its own advantages and disadvantages. The main advantage of the theoretical and inviscid-flow methods is their low computational costs relative to CFD. This becomes important when low-cost estimates are necessary, for example, for real-time control and maneuvering of bio-inspired swimmers, or for optimization studies in which a large parameter space needs to be investigated to identify why some biological features have evolved in nature, i.e., if these features evolved in ways that optimized a function such as acceleration or energy efficiency during unsteady swimming. However, the results from these methods need to be closely examined to ensure that their simplifying assumptions does not affect the conclusions. The main simplifying assumption of the EBT and vortex-panel methods is the assumption of inviscid flow, which ignores the boundary layer, and cannot capture flow separation, vortex-shedding, and the interaction of the shed vortices in the wake. Therefore, one area of recent interest is developing reduced-order models that improve the estimate of EBT or inviscid-vortex methods. CFD techniques do not have the above simplifying assumptions, and can provide detailed information on the 3D flow and pressure fields. They are particularly suitable for complementing experiments of unsteady locomotion in which the body shape, motion, and flow at a few planes are measured. The body shape and motion are used as input to the numerical simulations to obtain the 3D flow field, which can be validated against the measured flow field. The validated simulations can provide different parameters of swimming

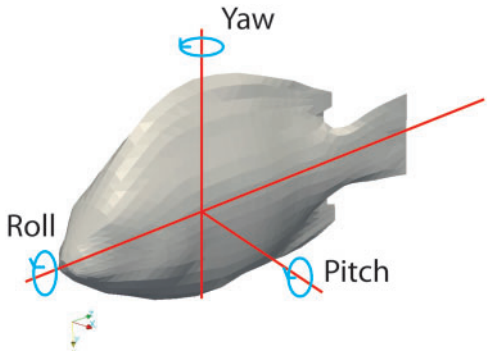

Fig. 5 The angles of roll, pitch, and yaw for a fish. During the C-start, the sunfish rotates around the yaw axis but not around the roll or pitch axes. The erection of the fins increases the moment of inertia around the roll and pitch axes, but not around the yaw axis. Taken from Borazjani (2013). (This figure is available in black and white in print and in color at *Integrative and Comparative Biology* online.)

performance such as force, power, and efficiency based on the 3D flow and pressure fields, which, as discussed in the Fast-starts and turning maneuvers section (Fig. 3), is required to correctly estimate these parameters for unsteady swimming.

The main limitation of current simulations is the computational cost that has restricted them to lower Re regimes, two-dimensions, or the limit of inviscid flow (Wolfgang et al. 1999; Borazjani et al. 2012; Gazzola et al. 2012, 2014; Borazjani 2013; Li et al. 2014). This is due to the fact that the computational cost increases with the increase of the Re, because as the Re increases the smallest eddies in the turbulent-flow regime, called the Kolmogorov scale, become smaller. As the Kolmogorov scale becomes smaller the grid needs to be refined to resolve the smaller scales. This increases the computational cost drastically as Re is increased, which makes direct numerical simulations quite challenging, if not impossible, at the typical Re at which most adult fish swim ($Re > 10^5$). To carry out simulations at realistic Re, modeling of turbulence is needed. Turbulence models based on Reynolds-averaged Navier–Stokes equations are too dissipative and not good candidates to model unsteady aquatic locomotions. Large-eddy simulation is a numerical technique in which only the large eddies are resolved and the small eddies, which mainly dissipate energy, are modeled (sub-grid scale model). Therefore, larger grid size, which only resolve the larger eddies, can be used to reduce the cost of numerical simulations at high Re. The large-eddy simulation with a simple sub-grid scale model has recently been implemented in the immersed-boundary method (Kang et al. 2012), and applied to swimming (Borazjani and Daghooghi 2013). Even in simulations of large eddies the resolution of the grid near the moving body needs to be refined to capture the thin boundary layer. To reduce the computational costs the resolution of the grid can be refined locally, using static (Li et al. 2012; Borazjani et al. 2013) or dynamic refinement of the grid (Tytell et al. 2010; Gazzola et al. 2014). Such methods show good promise for use in simulating unsteady aquatic locomotion.

The insights obtained through theoretical and computational work were discussed in the Insights from theoretical and computational studies section. The active control of anal and dorsal fins during C-start was hypothesized in the Fast-starts and turning maneuvers section to be related to the stability of sunfish. In fact, the stability of aquatic swimmers during unsteady swimming is an area that needs further investigation. Numerical simulations can help in understanding the mechanisms of stability that fish use during unsteady locomotion, e.g., by quantifying the torque, moment of inertia; motion around the axes of yaw, roll, and pitch; and the contribution/effect of the fins and their erection/movements on these quantities during unsteady maneuvers.

References

Angot P, Bruneau C-H, Fabrie P. 1999. A penalization method to take into account obstacles in incompressible viscous flows. Numer Math 81:497–520.

Bergstrom C. 2002. Fast-start swimming performance and reduction in lateral plate number in threespine stickleback. Can J Zool 80:207–13.

Bhalla APS, Bale R, Griffith BE, Patankar NA. 2013. A unified mathematical framework and an adaptive numerical method for fluid-structure interaction with rigid, deforming, and elastic bodies. J Comput Phys 250:446–76.

Blake R. 1983. Functional design and burst-and-coast swimming in fishes. Can J Zool 61:2491–4.

Blake R, Chatters L, Domenici P. 1995. Turning radius of yellowfin tuna (*Thunnus albacares*) in unsteady swimming manoeuvres. J Fish Biol 46:536–8.

Borazjani I. 2013. The functional role of caudal and anal/dorsal fins during the C-start of a bluegill sunfish. J Exp Biol 216:1658–69.

Borazjani I, Sotiropoulos F. 2010. On the role of form and kinematics on the hydrodynamics of body/caudal fin swimming. J Exp Biol 213:89–107.

Borazjani I, Daghooghi M. 2013. The fish tail motion forms an attached leading edge vortex. Proc R Soc B 280:20122071.

Borazjani I, Ge L, Sotiropoulos F. 2008. Curvilinear immersed boundary method for simulating fluid structure interaction with complex 3D rigid bodies. J Comput phys 227:7587–620.

Borazjani I, Sotiropoulos F, Malkiel E, Katz J. 2010. On the role of copepod antenna in the production of hydrodynamic force during hopping. J Exp Biol 213:3019–35.

Borazjani I, Sotiropoulos F, Tytell ED, Lauder GV. 2012. Hydrodynamics of the bluegill sunfish c-start escape response: three-dimensional simulations and comparison with experimental data. J Exp Biol 215:671–84.

Borazjani I, Ge L, Le T, Sotiropoulos F. 2013. A parallel overset-curvilinear-immersed boundary framework for simulating complex 3D incompressible flows. Comput Fluids 77:76–96.

Burnett NJ, Hinch SG, Braun DC, Casselman MT, Middleton CT, Wilson SM, Cooke SJ. 2014. Burst swimming in areas of high flow: delayed consequences of anaerobiosis in wild adult sockeye salmon. Physiol Biochem Zool 87:587–98.

Canfield JG, Rose GJ. 1993. Activation of Mauthner neurons during prey capture. J Comp Physiol A 172:611–8.

Chadwell BA, Ashley-Ross MA. 2012. Musculoskeletal morphology and regionalization within the dorsal and anal fins of bluegill sunfish (*Lepomis macrochirus*). J Morphol 273:405–22.

Chadwell BA, Standen EM, Lauder GV, Ashley-Ross MA. 2012a. Median fin function during the escape response of bluegill sunfish (*Lepomis macrochirus*). I: Fin-ray orientation and movement. J Exp Biol 215:2869–80.

Chadwell BA, Standen EM, Lauder GV, Ashley-Ross MA. 2012b. Median fin function during the escape response of bluegill sunfish (*Lepomis macrochirus*). II: Fin-ray curvature. J Exp Biol 215:2881–90.

Coquerelle M, Cottet G-H. 2008. A vortex level set method for the two-way coupling of an incompressible fluid with colliding rigid bodies. J Comput Phys 227:9121–37.

Danos N, Lauder GV. 2012. Challenging zebrafish escape responses by increasing water viscosity. J Exp Biol 215:1854–62.

Domenici P, Blake RW. 1991. The kinematics and performance of the escape response in the angelfish (*Pterophyllum eimekei*). J Exp Biol 156:187.

Domenici P, Blake RW. 1993. Escape trajectories in angelfish (*Pterophyllum eimekei*). J Exp Biol 177:253.

Domenici P, Batty RS. 1997. Escape behaviour of solitary herring (*Clupea harengus*) and comparisons with schooling individuals. Mar Biol 128:29–38.

Domenici P, Blake R. 1997. The kinematics and performance of fish fast-start swimming. J Exp Biol 200:1165.

Domenici P, Standen EM, Levine RP. 2004. Escape manoeuvres in the spiny dogfish (*Squalus acanthias*). J Exp Biol 207:2339.

Donea J, Huera A, Ponthot J, Rodriguez-Ferran A. 2004. Arbitrary Lagrangian–Eulerian methods. In: Stein E, de Borst R, Hughes TJR, editors. Encyclopedia of computational mechanics. Somerset (NJ): John Wiley & Sons.

Eaton RC, Lee RKK, Foreman MB. 2001. The Mauthner cell and other identified neurons of the brainstem escape network of fish. Prog Neurobiol 63:467–85.

Eldredge JD. 2006. Numerical simulations of undulatory swimming at moderate Reynolds number. Bioinspir Biomim 1:S19.

Ellerby DJ, Altringham JD. 2001. Spatial variation in fast muscle function of the rainbow trout *Oncorhynchus mykiss* during fast-starts and sprinting. J Exp Biol 204:2239.

Fauci LJ, Peskin CS. 1988. A computational model of aquatic animal locomotion. J Comput Phys 77:85–108.

Fetcho JR. 1991. Spinal network of the Mauthner cell. Brain Behav Evol 37:298–316.

Fish FE, Nicastro AJ. 2003. Aquatic turning performance by the whirligig beetle: constraints on maneuverability by a rigid biological system. J Exp Biol 206:1649–56.

Frith H, Blake R. 1991. Mechanics of the startle response in the northern pike, *Esox lucius*. Can J Zool 69:2831–9.

Gazzola M, Van Rees WM, Koumoutsakos P. 2012. C-start: optimal start of larval fish. J Fluid Mech 1:1–14.

Gazzola M, Hejazialhosseini B, Koumoutsakos P. 2014. Reinforcement learning and wavelet adapted vortex methods for simulations of self-propelled swimmers. SIAM J Sci Comput 36:B622–39.

Gazzola M, Chatelain P, Van Rees WM, Koumoutsakos P. 2011. Simulations of single and multiple swimmers with non-divergence free deforming geometries. J Comput Phys 230:7093–114.

Gilmanov A, Sotiropoulos F. 2005. A hybrid Cartesian/immersed boundary method for simulating flows with 3D, geometrically complex, moving bodies. J Comput Phys 207:457–92.

Gray J. 1933. Studies in animal locomotion. I. The movement of fish with special reference to the eel. J Exp Biol 10:88–104.

Harper DG, Blake RW. 1988. Energetics of piscivorous predator–prey interactions. J Theor Biol 134:59–76.

Harper DG, Blake RW. 1989. On the error involved in high-speed film when used to evaluate maximum accelerations of fish. Can J Zool 67:1929–36.

Harper DG, Blake RW. 1991. Prey capture and the fast-start performance of northern pike *Esox lucius*. J Exp Biol 155:175–92.

Hess JL, Smith A. 1967. Calculation of potential flow about arbitrary bodies. Prog Aerospace Sci 8:1–138.

Jayne BC, Lauder GV. 1993. Red and white muscle activity and kinematics of the escape response of the bluegill sunfish during swimming. J Comp Physiol A 173:495–508.

Jayne BC, Lozada AF, Lauder GV. 1996. Function of the dorsal fin in bluegill sunfish: motor patterns during four distinct locomotor behaviors. J Morphol 228:307–26.

Ji H, Lien F-S, Yee E. 2008. A robust and efficient hybrid cut-cell/ghost-cell method with adaptive mesh refinement for moving boundaries on irregular domains. Comp Methods Appl Mech Eng 198:432–48.

Kang S, Borazjani I, Colby JA, Sotiropoulos F. 2012. Numerical simulation of 3D flow past a real-life marine hydrokinetic turbine. Adv Water Resour 39:33–43.

Kanso E. 2009. Swimming due to transverse shape deformations. J Fluid Mech 631:127–48.

Kanso E, Marsden JE, Rowley CW, Melli-Huber JB. 2005. Locomotion of articulated bodies in a perfect fluid. J Nonlinear Sci 15:255–89.

Katz J, Plotkin A. 2001. Low-speed aerodynamics. Cambridge, UK: Cambridge University Press.

Koumoutsakos P, Leonard A. 1995. High-resolution simulations of the flow around an impulsively started cylinder using vortex methods. J Fluid Mech 296:1–38.

Koyama M, Kinkhabwala A, Satou C, Higashijima S-I, Fetcho J. 2011. Mapping a sensory-motor network onto a structural and functional ground plan in the hindbrain. Proc Natl Acad Sci USA 108:1170–5.

Lauder GV, Anderson EJ, Tangorra J, Madden PGA. 2007. Fish biorobotics: kinematics and hydrodynamics of self-propulsion. J Exp Biol 210:2767.

Li G, Müller UK, van Leeuwen JL, Liu H. 2012. Body dynamics and hydrodynamics of swimming fish larvae: a computational study. J Exp Biol 215:4015–33.

Li G, Müller UK, van Leeuwen JL, Liu H. 2014. Escape trajectories are deflected when fish larvae intercept their own C-start wake. J R Soc Interface 11:20140848.

Lighthill MJ. 1960. Note on swimming of slender fish. J Fluid Mech 9:305.

Lighthill MJ. 1969. Hydromechanics of aquatic animal propulsion. Annu Rev Fluid Mech 1:413–46.

Lighthill MJ. 1970. Aquatic animal propulsion of high hydromechanical efficiency. J Fluid Mech 44:265–301.

Lighthill MJ. 1971. Large-amplitude elongated-body theory of fish locomotion. Proc R Soc Lond B 179:125–38.

Lomax H. 1960. Indicial aerodynamics. In: Jones WP, editor. Manual on aeroelasticity, Vol. 2. London: North Atlantic Treaty Organisation Advisory Group for Aeronautical Research and Development (AGARD). Ch. 6, p. 1–58.

Maresh JL, Fish FE, Nowacek DP, Nowacek SM, Wells RS. 2004. High performance turning capabilities during foraging by bottlenose dolphins (*Tursiops truncatus*). Mar Mamm Sci 20:498–509.

Mittal R, Iaccarino G. 2005. Immersed boundary methods. Annu Rev Fluid Mech 37:239–61.

Mittal R, Dong H, Bozkurttas M, Najjar F, Vargas A, von Loebbecke A. 2008. A versatile sharp interface immersed boundary method for incompressible flows with complex boundaries. J Comput Phys 227:4825–52.

Muller UK, Stamhuis EJ, Videler JJ. 2000. Hydrodynamics of unsteady fish swimming and the effects of body size: comparing the flow fields of fish larvae and adults. J Exp Biol 203:193–206.

Muller UK, van den Boogaart JGM, van Leeuwen JL. 2008. Flow patterns of larval fish: undulatory swimming in the intermediate flow regime. J Exp Biol 211:196–205.

Muller UK, Van Den Heuvel BLE, Stamhuis EJ, Videler JJ. 1997. Fish foot prints: morphology and energetics of the wake behind a continuously swimming mullet (*Chelon labrosus Risso*). J Exp Biol 200:2893–906.

Muller UK, Smit J, Stamhuis EJ, Videler JJ. 2001. How the body contributes to the wake in undulatory fish swimming: flow fields of a swimming eel (*Anguilla anguilla*). J Exp Biol 204:2751–62.

Nauen JC, Lauder GV. 2002. Hydrodynamics of caudal fin locomotion by chub mackerel, *Scomber japonicus* (Scombridae). J Exp Biol 205:1709–24.

Niiler P, White H. 1969. Note on the swimming deceleration of a dolphin. J Fluid Mech 38:613–617.

Parson JM, Fish FE, Nicastro AJ. 2011. Turning performance of batoids: Limitations of a rigid body. J Exp Mar Biol Ecol 402:12–8.

Peskin CS. 1972. Flow patterns around heart valves: a numerical method. J Comput Phys 10:252–71.

Peskin CS. 1977. Numerical analysis of blood flow in the heart. J Comput Phys 25:220.

Peskin CS, McQueen DM. 1980. Modeling prosthetic heart valves for numerical analysis of blood flow in the heart. J Comput Phys 37:113–32.

Peskin CS, McQueen DM. 1989. A three-dimensional computational method for blood flow in the heart. 1. Immersed elastic fibers in a viscous incompressible fluid. J Comput Phys 81:372–405.

Robinson A, Laurmann J. 1956. Wing theory. Cambridge, UK: Cambridge University Press.

Sethian JA. 1999. Level set methods and fast marching methods: evolving interfaces in computational geometry, fluid mechanics, computer vision, and materials science. Cambridge, UK: Cambridge University Press.

Spierts IL, Leeuwen JL. 1999. Kinematics and muscle dynamics of C-and S-starts of carp (*Cyprinus carpio* L.). J Exp Biol 202:393.

Standen EM, Lauder G. 2005. Dorsal and anal fin function in bluegill sunfish *Lepomis macrochirus*: three-dimensional kinematics during propulsion and maneuvering. J Exp Biol 208:2753–63.

Stöcker S, Weihs D. 2001. Optimization of energetic advantages of burst swimming of fish. Math Methods Appl Sci 24:1387–400.

Strickler JR. 1975. Swimming of planktonic *Cyclops* species (Copepoda, Crustacea): pattern, movements and their control. In: Wu TY, Brokaw CJ, Brennen CE, editors. Swimming and flying in nature, Vol. 2. New York: Plenum Pub Corp. p. 599–613.

Tytell ED. 2004. Kinematics and hydrodynamics of linear acceleration in eels, *Anguilla rostrata*. Proc R Soc B Biol Sci 271:2535–40.

Tytell ED, Lauder GV. 2002. The C-start escape response of *Polypterus senegalus*: bilateral muscle activity and variation during stage 1 and 2. J Exp Biol 205:2591.

Tytell ED, Lauder GV. 2004. The hydrodynamics of eel swimming I. Wake structure. J Exp Biol 207:1825–41.

Tytell ED, Lauder GV. 2008. Hydrodynamics of the escape response in bluegill sunfish, *Lepomis macrochirus*. J Exp Biol 211:3359.

Tytell ED, Hsu C-Y, Williams TL, Cohen AH, Fauci LJ. 2010. Interactions between internal forces, body stiffness, and fluid environment in a neuromechanical model of lamprey swimming. Proc Natl Acad Sci USA 107:19832–7.

van Duren LA, Videler JJ. 2003. Escape from viscosity: the kinematics and hydrodynamics of copepod foraging and escape swimming. J Exp Biol 206:269.

van Rees WM, Gazzola M, Koumoutsakos P. 2013. Optimal shapes for anguilliform swimmers at intermediate Reynolds numbers. J Fluid Mech 722:R3.

Videler J, Weihs D. 1982. Energetic advantages of burst-and-coast swimming of fish at high speeds. J Exp Biol 97:169–78.

Videler JJ, Hess F. 1984. Fast continuous swimming of two pelagic predators, saithe (*Pollachius virens*) and mackerel (*Scomber scombrus*): a kinematic analysis. J Exp Biol 109:209–28.

Wakeling JM, Johnston I. 1998. Muscle power output limits fast-start performance in fish. J Exp Biol 201:1505.

Wakeling JM, Johnston IA. 1999. Predicting muscle force generation during fast-starts for the common carp *Cyprinus carpio*. J Comp Physiol B Biochem Syst Environ Physiol 169:391–401.

Wakeling JM, Kemp KM, Johnston IA. 1999. The biomechanics of fast-starts during ontogeny in the common carp *Cyprinus carpio*. J Exp Biol 202:3057.

Walker JA. 1998. Estimating velocities and accelerations of animal locomotion: a simulation experiment comparing numerical differentiation algorithms. J Exp Biol 201:981–95.

Walker JA, Ghalambor CK, Griset OL, McKenney D, Reznick DN. 2005. Do faster starts increase the probability of evading predators? Funct Ecol 19:808–15.

Webb P. 1977. Effects of median-fin amputation on fast-start performance of rainbow trout (*Salmo gairdneri*). J Exp Biol 68:123.

Webb P, Skadsen J. 1980. Strike tactics of Esox. Can J Zool 58:1462–9.

Webb PW. 1984. Body and fin form and strike tactics of four teleost predators attacking fathead minnow (*Pimephales promelas*) prey. Can J Fish Aquat Sci 41:157–65.

Webb PW, LaLiberte GD, Schrank AJ. 1996. Does body and fin form affect the maneuverability of fish traversing vertical and horizontal slits? Environ Biol Fish 46:7–14.

Weihs D. 1972. A hydrodynamical analysis of fish turning manoeuvres. Proc R Soc B 182:59–72.

Weihs D. 1973. The mechanism of rapid starting of slender fish. Biorheology 10:343.

Westneat MW, Hale ME, McHenry MJ, Long JH. 1998. Mechanics of the fast-start: muscle function and the role of intramuscular pressure in the escape behavior of *Amia calva* and *Polypterus palmas*. J Exp Biol 201:3041.

Wilson R, Lefrançois C, Domenici P, Johnston I. 2010. Environmental influences on unsteady swimming behaviour: consequences for predator–prey and mating encounters in teleosts. In: Domenici P, Kapoor BG, editors. Fish locomotion: An eco-ethological perspective. Enfield (NH): Science Publishers. p. 269–95.

Wolfgang MJ, Anderson JM, Grosenbaugh MA, Yue DK, Triantafyllou MS. 1999. Near-body flow dynamics in swimming fish. J Exp Biol 202:2303–27.

Wu TY-T. 1960. Swimming of a waving plate. J Fluid Mech 10:321.

Wu TY-T. 1971a. Hydromechanics of swimming propulsion. Part 1. Swimming of a two-dimensional flexible plate at variable forward speeds in an inviscid fluid. J Fluid Mech 46:337.

Wu TY-T. 1971b. Hydromechanics of swimming propulsion. Part 2. Some optimum shape problems. J Fluid Mech 46:521.

Wu TY-T. 1971c. Hydromechanics of swimming propulsion. Part 3. Swimming and optimum movements of slender fish with side fins. J Fluid Mech 46:545–68.

Wu TY. 2011. Fish swimming and bird/insect flight. Annu Rev Fluid Mech 43:25–58.

Yen J, Strickler JR. 1996. Advertisement and concealment in the plankton: what makes a copepod hydrodynamically conspicuous? Invert Biol 115:191–205.

Zottoli SJ, Bentley AP, Prendergast BJ, Rieff HI. 1995. Comparative studies on the Mauthner cell of teleost fish in relation to sensory input. Brain Behav Evol 46:151–64.